Simultaneous measurement of thermal diffusivity and optical absorption coefficient using photothermal radiometry. I. Homogeneous solids

Raquel Fuente, Estibaliz Apiñaniz, Arantza Mendioroz, and Agustín Salazar[a)]
Departamento de Física Aplicada I, Escuela Técnica Superior de Ingeniería, Universidad del País Vasco, Alameda Urquijo s/n, Bilbao 48013, Spain

(Received 7 April 2011; accepted 11 June 2011; published online 9 August 2011)

Modulated photothermal radiometry (PTR) has been widely used to measure the thermal diffusivity of bulk materials. The method is based on illuminating the sample with a plane light beam and measuring the infrared emission with an infrared detector. The amplitude and phase of the PTR voltage is recorded as a function of the modulation frequency and then fitted to the theoretical model. In this work, we test the ability of modulated PTR to retrieve simultaneously the thermal diffusivity and the optical absorption coefficient of homogeneous slabs. In order to eliminate the instrumental factor, self-normalization is used, i.e., the ratio of the PTR signal recorded at the rear and front surfaces. The influence of the multiple reflections of the light beam, the heat losses, and the transparency to infrared wavelengths are analyzed. Measurements performed on a wide variety of homogeneous materials, covering the whole range from transparent to opaque, confirm the validity of the method. In Part II of this work, the method is extended to multilayered materials. © *2011 American Institute of Physics*. [doi:10.1063/1.3614524]

I. INTRODUCTION

In photothermal radiometry (PTR), the sample is excited by a light beam and its thermal emission is recorded by an infrared (IR) detector.[1–4] If the detector is a monolithic IR sensor, the technique is known as photothermal radiometry, while infrared thermography is used if the detector is made of an array of IR sensors. On the other hand, the technique is named modulated (lock-in) or pulsed according to the time dependence of the exciting light beam impinging the sample.

Modulated (or frequency domain) PTR consists of illuminating the sample by an intensity modulated light beam and detecting the oscillating component of the temperature rise by means of an infrared detector connected to a lock-in amplifier. As the temperature rise depends on the thermal properties of the sample, modulated PTR has been widely used to measure the thermal diffusivity of a large variety of materials.[5–11] In addition, using a focused (defocused) laser beam, the in-plane (through-thickness) thermal diffusivity of anisotropic materials can be obtained.[12]

Moreover, some photothermal techniques (photoacoustics spectroscopy or mirage effect) have proven to be very accurate in measuring the optical absorption coefficient of gases, liquids, and solids. These techniques compete with success against optical techniques in the case of weakly or highly absorbing materials.[13–15]

In modulated PTR with plane illumination, the amplitude and phase of the PTR voltage is recorded as a function of the modulation frequency and then fitted to the theoretical model. However, normalization procedures are needed in order to suppress the instrumental factor, i.e., the dependence of the detection electronics (IR detector, preamplifier, and lock-in amplifier) on frequency. Several normalization procedures have been proposed: (a) self-normalization, which consists of dividing the PTR signals recorded at the rear and front surfaces,[16] (b) comparison with a reference material,[17] (c) obtaining the instrumental factor by impinging the laser beam directly on the IR detector, and (d) comparison of the PTR signal of the sample with and without a backing liquid.[9] After testing these normalization procedures, we have selected the self-normalization method, since it provides the highest signal to noise ratio and amplitude and phase contrast. However, this normalization is not useful for semi-infinite (very thick) samples.

The aim of this work is to test the ability of modulated PTR to retrieve simultaneously and accurately the optical absorption coefficient (α) and the thermal diffusivity (D) in homogeneous slabs. First, we have analyzed the theory of PTR signal generation, including some additional effects, as the multiple reflections of the exciting light beam at the sample surfaces, the influence of heat losses, and the transparency of the sample to IR wavelengths. Then, we have performed modulated PTR measurements on a wide variety of materials: opaque to visible and IR wavelengths, opaque to visible but semitransparent to IR, semitransparent to visible but opaque to IR, and semitransparent to visible and IR. This study establishes the conditions and limits to perform accurate α and D measurements using modulated PTR. In Part II, we extend this work to multilayered samples in order to retrieve α and D in each layer.

II. THEORY

Let us consider a semitransparent slab of thickness L, illuminated by a light beam of wavelength λ and intensity I_o modulated at a frequency f ($\omega = 2\pi f$). The geometry of the problem is shown in Fig. 1. According to the Beer-Lambert law, the light intensity inside the sample is

[a)]Author to whom correspondence should be addressed. Electronic mail: agustin.salazar@ehu.es.

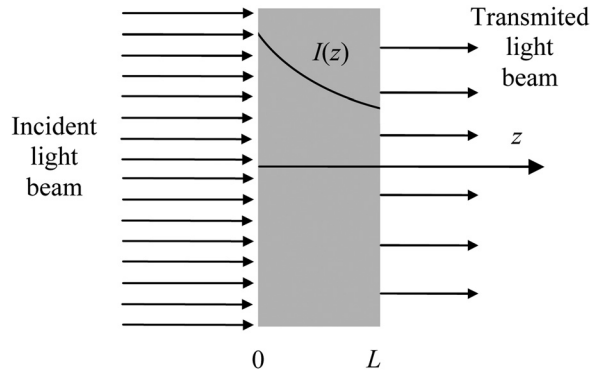

FIG. 1. Diagram of a semitransparent slab illuminated by a modulated light beam.

$I(z) = I_o(1-R)e^{-\alpha z}$, where R and α are the optical reflection and absorption coefficients of the slab at the wavelength of the light beam, respectively. The oscillating component of the temperature in the absence of heat losses is given by[18]

$$T(z) = \frac{I_o(1-R)\alpha^2}{2Kq(q^2-\alpha^2)} \left[\frac{(e^{-\alpha L}-e^{-qL})e^{qz} + (e^{-\alpha L}-e^{qL})e^{-qz} + \frac{q}{\alpha}(e^{qL}-e^{-qL})e^{-\alpha z}}{e^{qL}-e^{-qL}}\right], \quad (1)$$

where $q = \sqrt{i\omega/D}$ is the thermal wave vector and K and D are the thermal conductivity and thermal diffusivity of the sample, respectively.

For normalization purposes, we focus on the temperature ratio at the rear and front surfaces:

$$T_n = \frac{T(L)}{T(0)} = \frac{(e^{-\alpha L}-e^{-qL})e^{qL} + (e^{-\alpha L}-e^{qL})e^{-qL} + \frac{q}{\alpha}(e^{qL}-e^{-qL})e^{-\alpha L}}{2e^{-\alpha L} - e^{qL} - e^{-qL} + \frac{q}{\alpha}(e^{qL}-e^{-qL})}. \quad (2)$$

As can be seen, the self-normalized temperature depends on $L/\sqrt{D}$ and on αL, but does not depend on K and, therefore, both α and D can be retrieved simultaneously. Three main cases can be distinguished: (a) if the slab is opaque ($\alpha L \to \infty$) and thermally thick ($L/\sqrt{D} \to \infty$), Eq. (1) reduces to $T_n \approx 2e^{-qL}$, indicating that both the natural logarithm of the self-normalized temperature amplitude, $\mathrm{Ln}(T_n)$, and its phase, $\Psi(T_n)$, are parallel straight lines when plotted against $\sqrt{f}$, with a common slope $m = -L\sqrt{\pi/D}$. This equation provides a well-known method to measure the thermal diffusivity of opaque slabs.[19] (b) If the sample is transparent ($\alpha L \to 0$), Eq. (1) reduces to $T_n \approx 1$, indicating that both surfaces are at the same temperature. (c) For semitransparent samples, experimental results of the temperature ratio T_n must be fitted to Eq. (2). The three cases are shown in Fig. 2, where calculations have been performed for $D = 0.5$ mm^2/s and $L = 0.5$ mm. Note that, for the opaque case, the linear behavior only holds for $\sqrt{f} \geq 1.6$, i.e., when the material is thermally thick ($\mu \leq L/2$).

Figure 3 serves as an optical classification of a sample, depending on its α and L values. For $\alpha L < 0.8$, the sample is said to be transparent, indicating almost flat $\mathrm{Ln}(T_n)$ and $\Psi(T_n)$. In such a case, no information on its thermal and optical properties can be obtained from photothermal measurements. For $\alpha L > 10$ the sample behaves as opaque, indicating that both $\mathrm{Ln}(T_n)$ and $\Psi(T_n)$ are parallel straight lines when represented versus $\sqrt{f}$. In this case, only the thermal diffusivity of the sample can be obtained. For $0.8 < \alpha L < 10$, the sample is semitransparent and both α and D can be retrieved when fitting $\mathrm{Ln}(T_n)$ and $\Psi(T_n)$ to Eq. (2). It is worth mentioning that the transition between the three regions is not abrupt, and the values $\alpha L = 0.8$ and $\alpha L = 10$ are soft barriers. Note that the same slab can vary its classification depending on its thickness. In fact, a certain material can be classified as opaque, semitransparent, or transparent by appropriately selecting its thickness. For instance, a copper film 1 nm thick is transparent, while a glass slab 1 km thick is opaque. However, concerning the application of photothermal techniques, this thickness selection has severe restrictions. Actually, the

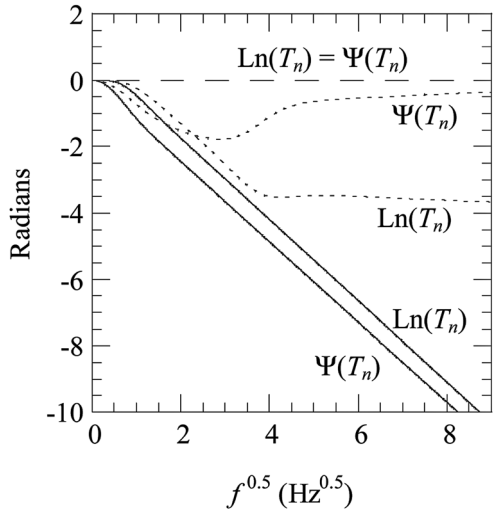

FIG. 2. Calculations of the natural logarithm of the amplitude and phase of the normalized temperature as a function of the square root frequency for a glass slab 0.5 mm thick ($D = 0.5$ mm^2/s). Three absorption coefficients have been considered: (a) continuous line, opaque material ($\alpha \to \infty$); (b) dashed line, transparent material ($\alpha \to 0$); and (c) dotted line, semitransparent material ($\alpha = 8$ mm^{-1}).

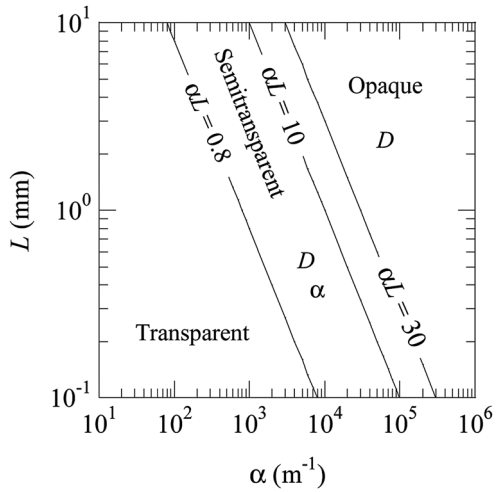

FIG. 3. Optical classification of solids according to the pair (α,L).

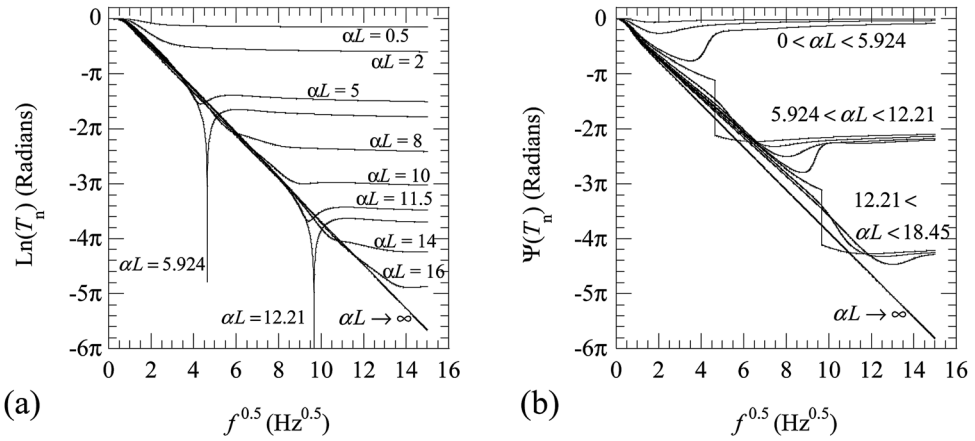

FIG. 4. Behavior of the natural logarithm of the amplitude (a) and phase (b) of the normalized temperature of semitransparent slabs as a function of the square root frequency. Calculations have been performed for $L/\sqrt{D} = 0.7\text{s}^{0.5}$, with increasing values of αL.

thickness must range between 0.2–4 mm in order to have a good signal to noise ratio together with a high enough amplitude and phase contrast.

The range $0.8 < \alpha L < 10$ seems very restrictive, but we have to remind that the transmission is given by $\tau = e^{-\alpha L}$. This means that this method allows us to measure the optical properties of samples with transmissions ranging from 0.5 down to 4×10^{-5}.

Note that, for $10 < \alpha L < 30$, $\text{Ln}(T_n)$ and $\Psi(T_n)$ are almost straight lines (see, for instance, the behavior for $\alpha L = 14$ and 16 in Fig. 4), since the curved part appears at high frequencies, where the photothermal signal is so small that these frequencies are not usable. However, these straight lines are not parallel, and only the slope of $\text{Ln}(T_n)$ must be used to obtain D.

In Fig. 4, we analyze, in detail, the evolution of $\text{Ln}(T_n)$ and $\Psi(T_n)$ as a function of $\sqrt{f}$ for a sample with $L/\sqrt{D} = 0.7\text{s}^{0.5}$. Different values of αL are considered, from zero (transparent) to infinity (opaque). As can be seen, for $\alpha L = 5.9243$, 12.211, 18.455, …, the amplitude of the normalized temperature goes to zero (the sharp dips in Fig. 4(a)). These αL values correspond to the solutions of the transcendent equation: $\{\text{Re}(T_n) = 0, \text{Img}(T_n) = 0\}$, where Re is the real part and Img is the imaginary part. It is worth mentioning that these αL values are independent of D. Those sharp dips are produced at frequencies satisfying $\alpha\mu = 1$, i.e., equal thermal diffusion length and optical penetration depth. Figure 4(b) shows the behavior of the normalized phase. As can be seen, at high frequencies, it converges to different asymptotic values depending on the αL value: to zero for $\alpha L < 5.9243$, to -2π for $5.9243 < \alpha L < 12.211$, to -4π for $12.211 < \alpha L < 18.455$, etc.

Now, we analyze some additional effects modifying the temperature distribution inside the slab and/or the signal recorded by the infrared detector in a modulated photothermal radiometry setup.

A. Multiple reflections of the incident light

If the incident light crossing the sample reaches the rear surface before vanishing it will be reflected back and forth, contributing to increase the sample temperature. Accounting for the multiple reflections of the light beam inside the slab of thickness L, the intensity distribution can be written as

$$I(z) = \frac{I_o(1-R)(e^{-\alpha z} + Re^{-2\alpha L}e^{\alpha z})}{1 - R^2 e^{-2\alpha L}}. \tag{3}$$

Then, proceeding as in Ref. 18, the sample temperature is obtained:

$$T(z) = \frac{I_o(1-R)\alpha^2}{2Kq(q^2-\alpha^2)} \left[\frac{(e^{-\alpha L} - e^{-qL})e^{qz} + (e^{-\alpha L} - e^{qL})e^{-qz} + \frac{q}{\alpha}(e^{qL} - e^{-qL})e^{-\alpha z}}{e^{qL} - e^{-qL}}\right] - \frac{I_o(1-R)\alpha^2 R e^{-2\alpha L}}{2Kq(q^2-\alpha^2)} \left[\frac{(e^{-qL} - e^{\alpha L})e^{qz} + (e^{qL} - e^{\alpha L})e^{-qz} + \frac{q}{\alpha}(e^{qL} - e^{-qL})e^{\alpha z}}{e^{qL} - e^{-qL}}\right], \tag{4}$$

where the second term is the correction with respect to Eq. (1). Note that when $L \to \infty$, Eq. (3) reduces to Eq. (1) since $e^{-2\alpha L} \to 0$. From Eq. (4), the normalized temperature $T_n = T(L)/T(0)$ is obtained. In Fig. 5, we show the effect of multiple reflections on the normalized temperature for the same glass slab of Fig. 2, with $R = 0.04$ (corresponding to normal incidence on a typical glass with a refraction index of 1.5) and $\alpha = 2\ \text{mm}^{-1}$, i.e., $\alpha L = 1$. Although the contribution of the multiple reflections is small, it must be taken into account in order to retrieve accurate α and D values. However, numerical calculations indicate that this effect is significant only for samples with $\alpha L < 2$.

B. Effect of heat losses

Eqs. (1) and (4) have been obtained by assuming adiabatic boundary conditions at the sample surfaces, i.e., absence of heat losses. However, it is expected that conduction to the surrounding gas as well as convection and radiation modify the temperature field of the sample, mainly at low frequencies. We have solved the heat diffusion equation with non-adiabatic boundary conditions (see the second part of

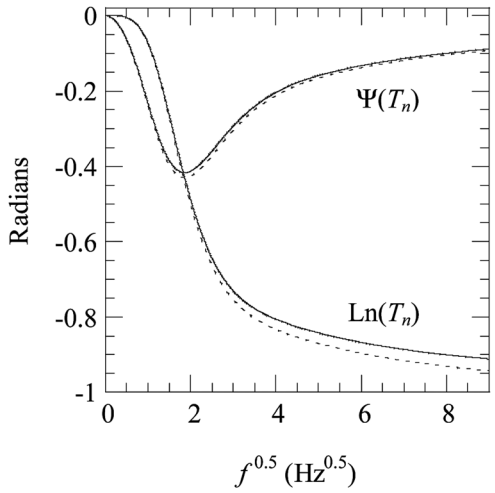

FIG. 5. Calculations of $\mathrm{Ln}(T_n)$ and $\Psi(T_n)$ as a function of $\sqrt{f}$ for a glass slab with $D=0.5$ mm^2/s, $L=0.5$ mm, $R=0.04$, and $\alpha=2$ mm^{-1}. Continuous lines correspond to the calculations without multiple reflections and dotted lines to those with multiple reflections of the exciting light beam.

this paper), and the result indicates that both the front $T(0)$ and rear $T(L)$ surface temperatures are affected by heat losses at low frequencies. However, the self-normalized temperature T_n is not affected, since the ratio $T(L)/T(0)$ completely compensates the effect of heat losses. Note that, at low frequencies, both $\mathrm{Ln}(T_n)$ and $\Psi(T_n)$ go to zero. Therefore, we can conclude that the effect of heat losses is negligible.

C. Transparency to the infrared radiation

The modulated voltage produced by the infrared detector is proportional to the oscillating surface temperature only if the sample is completely opaque to infrared wavelengths (in the case of HgCdTe detectors from 2 to 12 μm). This condition is fulfilled for metals and alloys, but not for most glasses and polymers. Actually, the visual appearance is not a reference to predict the infrared behavior. For instance, Ge is opaque for visible wavelengths, but completely transparent above 2 μm. Besides, some metallic oxides look black, but they are translucent at infrared wavelengths. In consequence, it is necessary to evaluate the influence of the transparency to the infrared wavelengths on the measured voltage.

If the sample is semitransparent to the infrared spectrum, the signal recorded by the infrared detector comes, not only from the sample surface, but from the whole sample. If we define β as the effective infrared absorption coefficient for the sample (averaging the sample behavior from 2 to 12 μm),[20] the signal recorded by the detector placed in front of the illuminated surface is given by[21]

$$S(0) = C\int_0^L \beta e^{-\beta z} T(z)dz, \tag{5}$$

where C is a constant that includes the emissivity of the sample, the sensor area and detectivity, and the temperature derivative of the Plank function at room temperature. $T(z)$ is the slab temperature given by Eq. (1). This means that we are assuming that heat losses associated to the infrared emission from the sample are so small that they do not affect the temperature field (note that this assumption holds for the oscillating temperature, but not for the dc temperature rise of the slab, which is highly limited by heat losses[22]). Similarly, the signal recorded by the detector placed in front of the non-illuminated surface is given by

$$S(L) = C\int_0^L \beta e^{\beta(z-L)} T(z)dz. \tag{6}$$

By substituting Eq. (1) into Eqs. (5) and (6) and solving the integrals analytically, the normalized signal is obtained

$$S_n = \frac{S(L)}{S(0)} = \frac{A}{B}e^{-\beta L}, \tag{7}$$

where A and B are given by

$$A = \frac{e^{-\alpha L}-e^{-qL}}{-(q+\beta)}\left(1-e^{(q+\beta)L}\right) + \frac{e^{-\alpha L}-e^{qL}}{q-\beta}\left(1-e^{(\beta-q)L}\right) + \frac{q}{\alpha}\frac{e^{qL}-e^{-qL}}{\alpha-\beta}\left(1-e^{(\beta-\alpha)L}\right), \tag{8a}$$

$$B = \frac{e^{-\alpha L}-e^{-qL}}{\beta-q}\left(1-e^{(q-\beta)L}\right) + \frac{e^{-\alpha L}-e^{qL}}{q+\beta}\left(1-e^{-(q+\beta)L}\right) + \frac{q}{\alpha}\frac{e^{qL}-e^{-qL}}{\alpha+\beta}\left(1-e^{-(\alpha+\beta)L}\right). \tag{8b}$$

In Fig. 6, we show the effect of the infrared transparency on the normalized signal S_n for the same glass slab of Fig. 2, with $\alpha=5$ mm^{-1} and different values of β ranging from 0 to ∞. Note that, even for an almost IR opaque material, with β values around 30 mm^{-1}, its influence on S_n is not negligible, mainly at the high frequency tail, and therefore, Eq. (7) must be used instead of Eq. (2). It is interesting to point out that, when exchanging the α and β values, the normalized signal S_n remains the same.

For fitting the experimental data, we will use a theoretical expression of the normalized PTR signal, combining the multiple reflections of the incident light and the transparency to the IR radiation

$$S_n = \frac{S(L)}{S(0)} = \frac{A+Re^{-2\alpha L}A1}{B+Re^{-2\alpha L}B1}e^{-\beta L}, \tag{9}$$

where $A1$ and $B1$ are given by

$$A1 = \frac{e^{\alpha L}-e^{-qL}}{-(q+\beta)}\left(1-e^{(q+\beta)L}\right) + \frac{e^{\alpha L}-e^{qL}}{q-\beta}\left(1-e^{(\beta-q)L}\right) + \frac{q}{\alpha}\frac{e^{qL}-e^{-qL}}{\alpha+\beta}\left(1-e^{(\alpha+\beta)L}\right), \tag{10a}$$

$$B1 = \frac{e^{\alpha L}-e^{-qL}}{\beta-q}\left(1-e^{(q-\beta)L}\right) + \frac{e^{\alpha L}-e^{qL}}{q+\beta}\left(1-e^{-(q+\beta)L}\right) + \frac{q}{\alpha}\frac{e^{qL}-e^{-qL}}{\alpha-\beta}\left(1-e^{(\alpha-\beta)L}\right). \tag{10b}$$

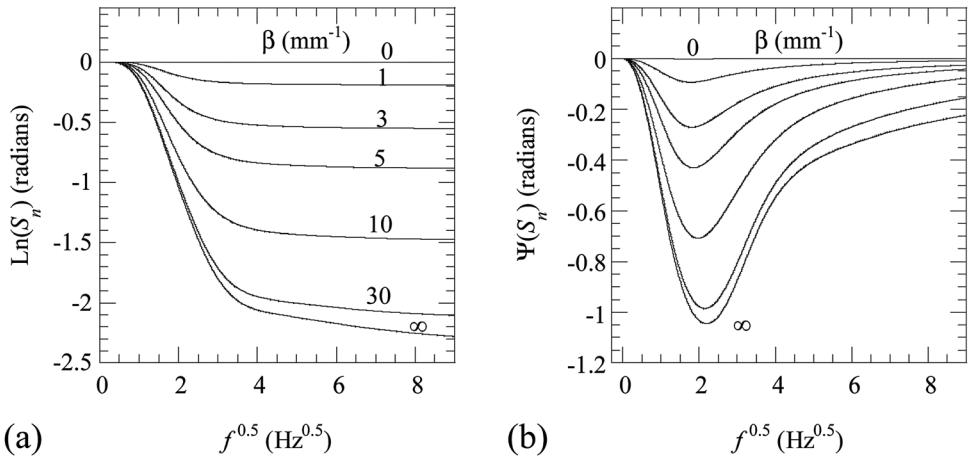

FIG. 6. Calculations of $\mathrm{Ln}(S_n)$ (a) and $\Psi(S_n)$ (b) as a function of $\sqrt{f}$ for a glass slab with $D=0.5$ mm^2/s, $L=0.5$ mm, $R=0.04$, and $\alpha=5$ mm^{-1}, and different values of β ranging from 0 (transparent to IR) to ∞ (opaque to IR).

III. EXPERIMENTAL RESULTS AND DISCUSSION

The experimental PTR setup is shown in Fig. 7. A solid state laser beam ($\lambda=532$ nm), modulated by an acousto-optic modulator, was used to heat the sample. The beam was expanded to a diameter of 1 cm to guarantee 1D heat propagation. Using plane mirrors, the laser was sent to the front or to the rear surface of the sample. The infrared radiation emitted from the sample was collected by an off-axis parabolic mirror system and detected by a HgCdTe sensor (2–12 μm). We have chosen an active area of 1 mm^2, since it has the highest product detectivity × area. The voltage produced by the detector was amplified and then fed into a digital lock-in amplifier. A Ge window, which is opaque for visible wavelengths but transparent from 2–12 μm, is usually placed in front of the detector to prevent the green light of the laser to reach the IR sensor. In this work, a Ge based spectral filter was used to reduce the transmission region of the detector (5–12 μm).

Several authors have pointed out that the measured PTR voltage is affected by coherent noise generated by stray-light heating the IR optics and cutoff filter.[23–25] However, they experimentally showed that this effect is only significant for modulation frequencies exceeding 1 kHz. As all the measurements in this work have been performed at frequencies far below this value, this coherent noise has not been considered in the fittings.

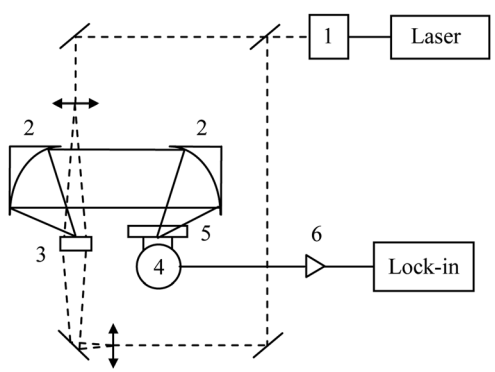

FIG. 7. Scheme of the experimental setup. 1. Acousto-optic modulator, 2. off-axis parabolic mirrors, 3. sample, 4. HgCdTe detector, 5. Ge window, 6. preamplifier.

In order to verify the ability of modulated PTR to characterize the thermal diffusivity and the absorption coefficient of solid slabs, we have performed measurements on a wide set of samples. They are summarized in Fig. 8 according to their optical properties. The experimental PTR measurements are shown in Fig. 9.

In Fig. 9(a), we show the results for two samples (vitreous carbon and carbon fiber reinforced (CFR) composite) that are opaque for visible and IR wavelengths. As can be seen, both $\mathrm{Ln}(S_n)$ (dots) and $\Psi(S_n)$ (crosses) are parallel and straight lines as a function of $\sqrt{f}$, except at low frequencies, where the material is thermally thin. In Table I, the thermal diffusivity values obtained from the slopes using the expression $m=-L\sqrt{\pi/D}$ for Ni, SiC (38% porosity), vitreous carbon, AISI-304 stainless steel, CFR composite, and poly-L-lactide (PLLA) composite are shown. They are in good agreement with literature values. In this method, there are three reliability criteria: (a) the parallelism of both straight lines, (b) the fit of the phase converging to 0 rads at $f=0$, and (c) a large range of linear behavior (about 5–6 rads) before noise appears. The thermal diffusivity underestimation for Ni and AISI-304 is due to the painting layers used to increase both the absorption to the laser light and the IR emission. The effect of these layers will be discussed in detail in the second part of this work.

The experimental result of a Ge slab 3 mm thick is also shown in Fig. 9(a). As this material is completely transparent at IR wavelengths, $\Psi(S_n)$ (crosses) is zero for all frequencies. Due to the different light intensity absorbed at both surfaces, $\mathrm{Ln}(S_n)$ (dots) is not zero, as it should be according to the theoretical model, but a constant value. No information on the thermal and optical properties of this material can be obtained.

In Fig. 9(b), we show the experimental results for a neutral density filter with $\alpha=2.33$ mm^{-1} at 532 nm (Cary spectrometer) that is opaque for IR wavelengths above 5 μm. Three slabs of different thicknesses have been measured to test the reliability of the results. The continuous lines are the fittings to Eq. (9). The same D and α values for the three samples are obtained (see Table I) inside the experimental uncertainty (5% and 10%, respectively). The data of Fig. 9(b) indicate that, if the sample is quite thick, the phase

	IR Opaque	IR Semitransparent	IR Transparent
Visible Opaque	Ni Porous SiC Vitreous carbon AISI-304 CFR composite PLLA composite *D*	$LaMnO_3$ NiO Cr_2O_3 CoO Si *D*,β	Ge ZnSe No contrast
Visible Semitransparent	ND filters paper *D*,α	Colored filters PEEK polymer *D*,α,β	PLLA polymer No contrast
Visible Transparent	BK7 glass No signal	MgF_2 sapphire No signal	CaF_2 No signal

FIG. 8. Optical classification of the materials measured in this work.

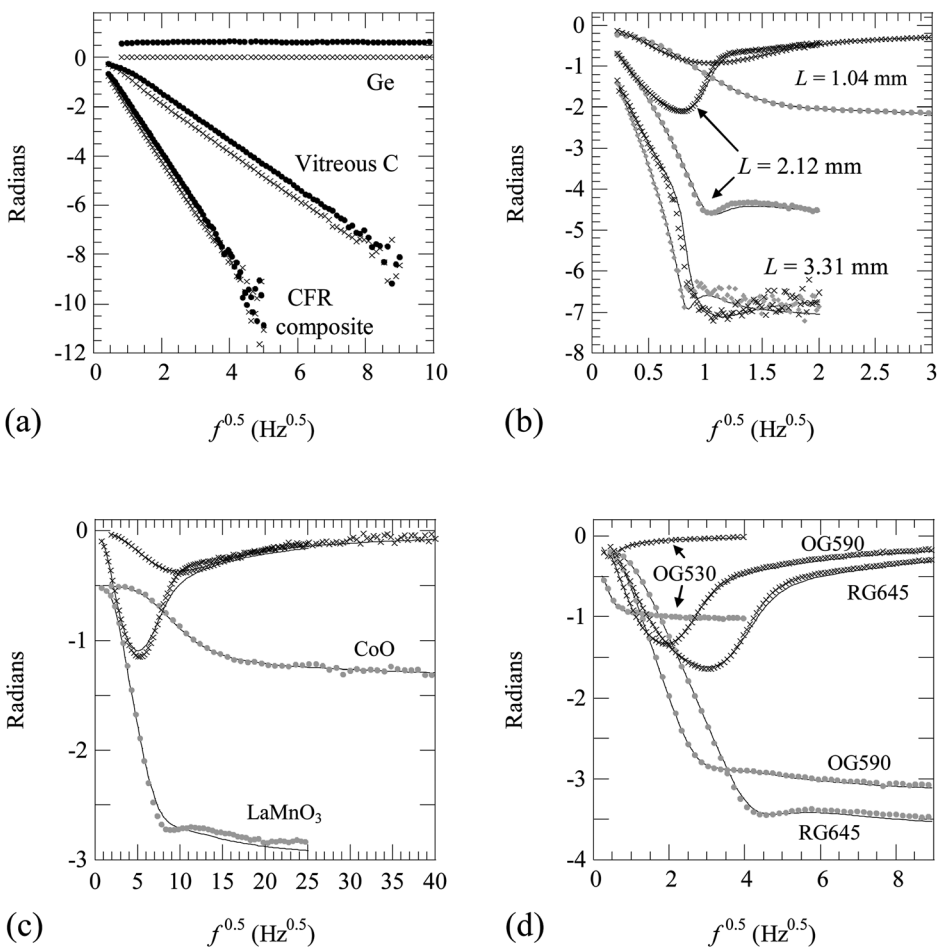

FIG. 9. Experimental values of $\mathrm{Ln}(S_n)$ (dots) and $\Psi(S_n)$ (crosses) for materials with different optical properties. (a) Visible and IR opaque sample, together with Ge that is transparent to IR. (b) A neutral density filter, opaque to IR, with three different thicknesses. (c) $LaMnO_3$ and CoO that are opaque to visible but semitransparent to IR. (d) Colored filters, which are semitransparent to visible and IR wavelengths. Continuous lines are the fittings to Eq. (9).

contrast is high, but the signal to noise is poor (noisy data), since the PTR voltage from the rear illumination measurements is very small (a few tens of μV). On the contrary, if the sample is too thin, the signal to noise ratio is high (noise free data), but the phase contrast is small (less than 1 rad in phase). In consequence, whenever the thickness of the sample under study can be selected, an intermediate thickness providing a good enough signal to noise ratio together with a quite high phase contrast (about 2 rads) is the best choice.

TABLE I. Thermal diffusivity (D), optical absorption coefficient (α), and IR absorption coefficient (β) of the materials measured in this work. Uncertainty in D is 5% and α is 10%.

Material	L (mm)	D (mm^2/s)	D Literature[a] (mm^2/s)	α (mm^{-1}) This work	α (mm^{-1}) Cary spectrometer	β (mm^{-1})
Ni	1.03	18	22	—	∞	∞
Porous SiC	1.63	7.2	8.0	—	∞	∞
Vitreous C	1.34	6.0	6.0	—	∞	∞
AISI-304	0.94	3.4	4.0	—	∞	∞
CFR composite	0.85	0.51	0.50	—	∞	∞
ND filter	3.31	0.59	0.5–0.6	2.05	2.33	∞
ND filter	2.12	0.57	0.5–0.6	2.10	2.33	∞
ND filter	1.04	0.54	0.5–0.6	2.10	2.33	∞
Schott NG 1	0.478	0.48	0.5–0.6	10.5	11.1	∞
Schott OG 530	2.20	0.51	0.5–0.6	0.27	0.38	19.0
Schott OG 550	1.75	0.55	0.5–0.6	1.70	1.62	13.0
Schott OG 570	0.538	0.50	0.5–0.6	4.80	4.82	32.0
Schott OG 590	0.645	0.51	0.5–0.6	5.00	5.31	49.0
Schott RG 610	0.611	0.50	0.5–0.6	5.85	6.18	27.0
Schott RG 630	0.400	0.39	0.5–0.6	9.60	9.97	50.0
$LaMnO_3$	0.313	1.07	1.15	∞	∞	8.50
CoO	0.204	2.4	2.2	∞	∞	4.50
PLLA composite	0.460	0.10	—	—	—	—
Paper	0.247	0.16	0.144	8.10	—	∞
Paper	0.370	0.14	0.144	6.77	—	∞
PEEK	0.688	0.18	0.19	4.32	—	19.8
Ge	3.0	—	35	—	∞	—

[a]References 9, 26–32.

In Fig. 9(c), we show the experimental results for two metallic oxides, $LaMnO_3$ and CoO, that are completely black, i.e., opaque at visible wavelengths. However, the shape of $\mathrm{Ln}(S_n)$ (dots) and $\Psi(S_n)$ (crosses) indicate that these materials are semitransparent at IR wavelengths. The results of the fittings are shown in Table I. The retrieved D values agree with the measurements performed using a photopyroelectric setup.[26,27]

Finally, we have measured six colored filters with increasingly optical absorption coefficient at 532 nm. The main difference with respect to the neutral density filters is that they are not completely opaque at IR wavelengths, so the experimental data must be fitted to Eq. (9) with three unknowns: D, α, and β. The results of the fitting are shown in Table I, while the experimental results for three of them are plotted in Fig. 9(d). Note that, for OG530, that is very transparent at 532 nm, we have used a quite thick slab (2.20 mm) in order to increase the phase contrast as much as possible, while keeping a good enough signal to noise ratio. Anyway, this sample is placed in the lowest limit of this method ($\alpha L \approx 0.8$). This is why the retrieved α value is the least accurate. However, it is worth noting that the D value is the same as for the other filters of the family, indicating that thermal diffusivity is obtained with higher accuracy than the absorption coefficient.

In Fig. 10(a), we show the experimental PTR data for a composite material whose matrix is PLLA and the fillers are carbon nanotubes (0.75%). As can be seen, both $\mathrm{Ln}(S_n)$ (dots) and $\Psi(S_n)$ (crosses) become flat at high frequencies, indicating that the sample is not completely opaque (i.e., it falls in the region $10 < \alpha L < 30$). However, a good fitting to Eq. (9) cannot be obtained, since the high frequency data are too noisy. According to the theory, we have only used the slope of $\mathrm{Ln}(S_n)$ to retrieve D, whose value is given in Table I.

In materials like paper or polyether-ether-ketone (PEEK), there is not only light absorption but light scattering as well. Accordingly, the Beer-Lambert law does not hold. This means that light propagation in turbid media must be used as the source term in the heat diffusion equation, instead of Eq. (3).[33,34] We have measured some white paper and PEEK sheets, and we have fitted the amplitude and phase data to Eq. (9). The results are shown in Fig. 10(b). In this case, the retrieved α is an effective value, combining both absorption and scattering processes inside the material. Although a more complete model should be used, the obtained D value is in good agreement with the literature values (see Table I).

As a final remark, let us make some considerations about the accuracy of the retrieved values of D and α. In the case of opaque materials (both to visible and IR wavelengths), the parallelism of the straight lines of $\mathrm{Ln}(S_n)$ and $\Psi(S_n)$ provides a good test of the reliability of the obtained value of D. Moreover, the thickness of the sample should be selected in such a way that the straight lines produce changes of more than 4 rads before the noise appears. If both conditions are fulfilled, the main source of error comes from the uncertainty in L (surface roughness, lack of parallelism, …). Accordingly, for opaque materials, we estimate the uncertainty in thermal diffusivity to be $\Delta D \leq 3\%$. For not

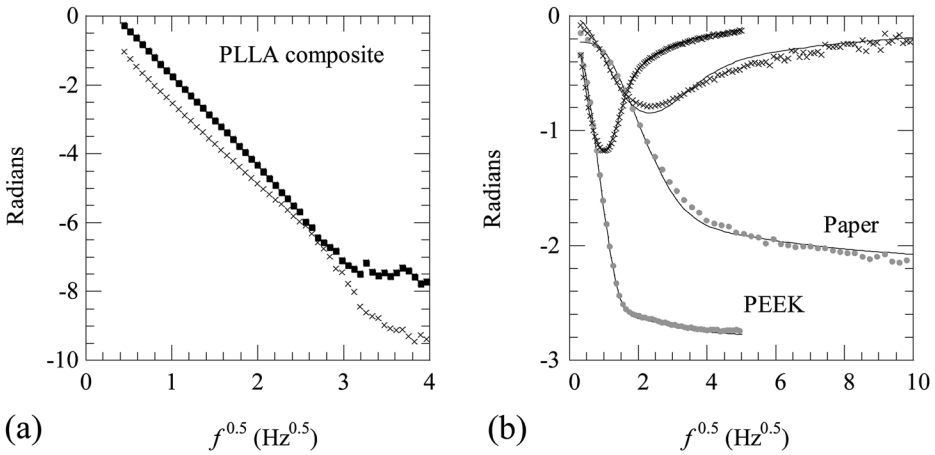

FIG. 10. Experimental values of Ln(S_n) (dots) and $\Psi(S_n)$ (crosses) for: (a) PLLA composite with 0.75% of carbon nanotubes, and (b) white paper and PEEK polymer.

completely opaque samples ($10 < \alpha L < 30$), only the slope of Ln(S_n) can be used to retrieve the thermal diffusivity of the sample. This means that the test of parallelism cannot be used, and we estimate the uncertainty in thermal diffusivity to raise up to $\Delta D \leq 5\%$. In the case of semitransparent samples ($0.8 < \alpha L < 10$), both D and α can be obtained, but the accuracy is not the same all along that range. At low αL values ($0.8 < \alpha L < 2$), the contrast in both Ln(S_n) and $\Psi(S_n)$ is small (see Fig. 4), reducing the accuracy of the retrieved D and α values. On the contrary, at high αL values ($7 < \alpha L < 10$), the contrast is high, but the signal is small, reducing the signal to noise ratio and, therefore, the accuracy of the obtained D and α values. The most accurate results are obtained for intermediate αL values ($4 < \alpha L < 6$), which produce a contrast between 2 to 4 rads, while keeping a good enough signal to noise ratio. Note that, in most cases, it is possible to work within this intermediate range by selecting the sample thickness appropriately. In this intermediate range, we estimate the errors in thermal diffusivity and optical absorption coefficient to be $\Delta D \leq 5\%$ and $\Delta\alpha \leq 10\%$. The main sources of error are the uncertainty in L, the effect of scattered light inside the sample, and, above all, that the model only takes into account an effective β value and not the complete IR spectrum from 5 to 12 μm. The reason for the uncertainty of α being higher than that of D is related to the fact that α is sensitive to the whole frequency scan of Ln(S_n) and $\Psi(S_n)$, while D is mainly sensitive to low frequencies, where the IR signal is higher.

IV. CONCLUSIONS

In this work, we have tested the ability of modulated PTR to measure simultaneously the thermal diffusivity and the optical absorption coefficient of homogeneous materials. The method is based on illuminating the sample with a plane light beam while recording the amplitude and phase of the PTR voltage as a function of the modulation frequency that are then fitted to the theoretical model. Self-normalization is used to suppress the instrumental factor. The effects of multiple reflections of the heating light beam as well as the transparency to infrared wavelengths have been included in the model.

For opaque samples (to visible and to IR wavelengths), the parallelism of the straight lines of Ln(S_n) and $\Psi(S_n)$ as a function of $\sqrt{f}$ guarantees the accuracy of the retrieved thermal diffusivity. For semitransparent samples (to visible and/or IR wavelengths), the fitting of Ln(S_n) and $\Psi(S_n)$ to the theoretical model gives α and D simultaneously. According to the theoretical and experimental results, α values in the range from 0.5 to 12 mm^{-1} can be retrieved. Whenever it is possible, the thickness of the sample should be selected in such a way that the phase contrast is between 1-2 rads. Below this value (low contrast) or above it (low signal to noise ratio), the accuracy decreases. If the sample is transparent to the exciting light beam or to the IR wavelengths, no information on the thermo-optical properties of the sample can be retrieved. The main drawback of this method is the exchangeable role of α and β, in such a way that it is not possible to distinguish between them. This issue can be overcome by performing several PTR measurements on the same sample, using heating lasers of different wavelength for each measurement. This procedure would give different α values while the β value remains constant.

According to the results of this work, modulated PTR appears as an appropriate tool to measure accurately and simultaneously the thermal diffusivity and the optical absorption coefficient of solids. Anyway, its powerfulness will be more evident when dealing with multilayered samples, which is the subject of Part II of this work.

ACKNOWLEDGMENTS

This work has been supported by the Ministerio de Ciencia e Innovación (MAT2008-01454).

[1]P. E. Nordal and S. O. Kanstad, Phys. Scr. **20**, 659 (1979).
[2]R. Santos and L. C. M. Miranda, J. Appl. Phys. **52**, 4194 (1981).
[3]R. D. Tom, E. P. O'Hara, and D. Benin, J. Appl. Phys. **53**, 5392 (1982).
[4]S. O. Kanstad and P. E. Nordal, Can. J. Phys. **64**, 1155 (1986).
[5]L. Fabbri and P. Fenici, Rev. Sci. Instrum. **66**, 3593 (1995).
[6]J. F. Bisson and D. Fournier, J. Appl. Phys. **83**, 1036 (1998).
[7]S. André, B. Rémy, D. Maillet, and A. Degiovanni, J. Appl. Phys. **96**, 2566 (2004).
[8]M. Broussely, A. P. Levick, and G. J. Edwards, Int. J. Thermophys. **26**, 221 (2005).

[9]M. Depriester, P. Hus, S. Delenclos, and H. Sahraoui, Rev. Sci. Instrum. **76**, 074902 (2005).
[10]C. Pradère, J. M. Goyhénèche, J. C. Batsale, S. Dilhaire, and R. Pailler, Int. J. Therm. Sci. **45**, 443 (2006).
[11]S. Trujillo, P. Martínez-Torres, P. Quintana, and J. J. Alvarado-Gil, Int. J. Thermophys. **31**, 805 (2010).
[12]A. Salazar, A. Sánchez-Lavega, A. Ocáriz, J. Guitonny, J. C. Pandey, D. Fournier, and A. C. Boccara, Appl. Phys. Lett. **67**, 626 (1995).
[13]G. C. Wetsel and F. A. McDonald, Appl. Phys. Lett. **30**, 252 (1977).
[14]Y. C. Teng and B. S. H. Royce, J. Opt. Soc. Am. **70**, 557 (1980).
[15]A. Mandelis, J. Appl. Phys. **54**, 3404 (1983).
[16]J. A. Balderas-López and A. Mandelis, Rev. Sci. Instrum. **74**, 5219 (2003).
[17]M. Munidasa, F. Funak, and A. Mandelis, J. Appl. Phys. **83**, 3495 (1998).
[18]A. Rosencwaig and A. Gersho, J. Appl. Phys. **47**, 64 (1976).
[19]M. Chirtoc, in *Thermal Wave Physics and Related Photothermal Tecniques: Basic Principles and Recent Developments*, edited by E. Marín (Transworld Research Network, Trivandrum, 2009), Chap. 2.
[20]B. Majaron and M. Milanič, Phys. Med. Biol. **53**, 255 (2008).
[21]H. G. Walther, U. Seidel, W. Karpen, and G. Busse, Rev. Sci. Instrum. **63**, 5479 (1992).
[22]A. Salazar, E. Apiñaniz, A. Mendioroz, and A. Oleaga, Eur. J. Phys. **31**, 1053 (2010).
[23]S. Paoloni and H. G. Walther, J. Appl. Phys. **82**, 101 (1997).
[24]S. Krueger, R. Kordecki, J. Pelzl, and B. K. Bein, J. Appl. Phys. **62**, 55 (1987).
[25]J. Bolte, J. H. Gu, and B. K. Bein, High Temp. - High Press. **29**, 567 (1997).
[26]A. Salazar, A. Oleaga, and D. Prabhakaran, Int. J. Thermophys. **25**, 1269 (2004).
[27]M. Massot, A. Oleaga, A. Salazar, D. Prabhakaran, M. Martin, P. Berthet, and G. Dhalenne, Phy. Rev. B **77**, 134438 (2008).
[28]L. R. Touloukian, R. W. Powell, C. Y. Ho, and M. C. Nicolasu, *Thermal Diffusivity* (IFI/Plenum, New York, 1973).
[29]D. P. Almond and P. M. Patel, *Photothermal Science and Techniques* (Chapman and Hall, London, 1996).
[30]Y. A. Çengel, *Heat Transfer: A Practical Approach* (McGraw-Hill, Boston, 2003).
[31]See http://www.goodfellow.com for more information about PEEK, AISI 304 and vitreous carbon.
[32]A. Sánchez-Lavega, A. Salazar, A. Ocáriz, L. Pottier, E. Gómez, L. M. Villar, and E. Macho, Appl. Phys. A **65**, 15 (1997).
[33]S. A. Prahl, A. Vitkin, U. Bruggemann, B. C. Wilson, and R. R. Anderson, Phys. Med. Biol. **37**, 1203 (1992).
[34]A. Matvienko, A. Mandelis, R. J. Jeon, and S. H. Abrams, J. Appl. Phys. **105**, 102022 (2009).